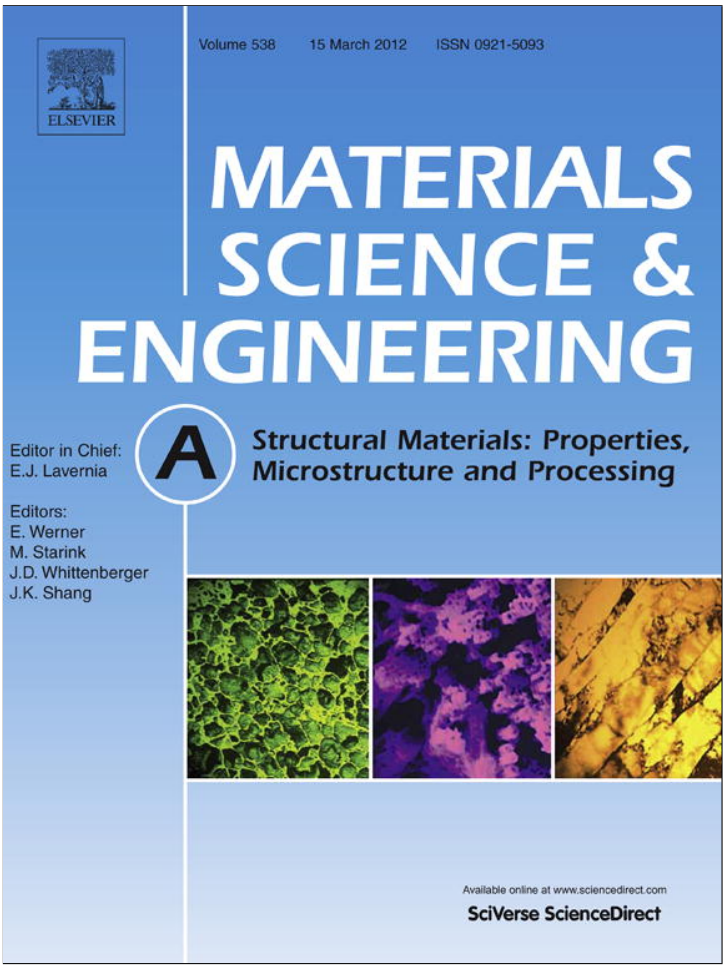

Materials Science and Engineering A 538 (2012) 272–280

Contents lists available at SciVerse ScienceDirect

Materials Science and Engineering A

journal homepage: www.elsevier.com/locate/msea

Precipitation microstructure and their strengthening effects of an Mg–2.8Nd–0.6Zn–0.4Zr alloy with a 0.2 wt.% Y addition

J.H. Li[a,b,1], G. Sha[a,c,*], W.Q. Jie[b], S.P. Ringer[a,c]

[a] Australian Centre for Microscopy and Microanalysis, The University of Sydney, Madsen Building F09, Sydney, NSW 2006, Australia
[b] State Key Laboratory of Solidification Processing, Northwestern Polytechnical University, Xi'an 710072, China
[c] ARC Centre of Excellence for Design in Light Metals, The University of Sydney, NSW 2006, Australia

ARTICLE INFO

Article history:
Received 3 October 2011
Received in revised form 10 January 2012
Accepted 11 January 2012
Available online 20 January 2012

Keywords:
Magnesium alloy
Precipitation
Mechanical properties
TEM
Atom probe tomography

ABSTRACT

A micro-alloy addition of Y (0.2 wt.%) produced a significant improvement in the tensile yield strength of an Mg–2.8Nd–0.6Zn–0.4Zr (wt.%) alloy at 200 °C, with a 28% increase from 143 MPa to 183 MPa. APT characterisation confirmed that small solute clusters in a high number density were present in the as-quenched sample. TEM examinations revealed that β-type precipitates habiting on prism $\{1\,1\,\bar{2}\,0\}$ planes were dominant in the sample after aged for 14 h at 200 °C, and they co-existed with γ-type precipitates on the basal plane of Mg matrix. The precipitation sequence of β-type precipitates is solute clusters → β″ → β′ → β_1 before the peak hardness. There was significant clustering of solutes in the Y-containing alloy, but Y did not clearly partition into clusters or precipitates and remained in the Mg matrix. β″, β′ and β_1 were measured with stoichiometric Mg_9(Nd,Zn), Mg_4(Nd,Zn) and Mg_2(Nd,Zn), respectively.

1. Introduction

Magnesium alloys have important applications in the automotive and aerospace industries because of their high specific strength for the weight reduction and better fuel economy [1]. However, the mechanical properties of conventional Mg alloys are often not suitable for high-temperature applications. The lower mechanical properties, particularly the lower tensile yield strength at elevated temperatures, hinder the wider application of Mg alloys [2]. The development of Mg alloys for the high-temperature application remains to be a challenging research target for the international materials community.

Rare-earth (RE) element addition has been considered to be effective to promote precipitation hardening and to improve the high-temperature performance of Mg alloys due to the formation of thermally stable nano-sized precipitates in a high number density [3–18]. Indeed, some commercial high-strength heat-resistant Mg alloys (i.e. WE54/43, QE22, etc.) contain at least two types of RE elements (one is main and the other is minor). Frequently, RE elements are selected from Nd, Y, sometimes Sc and Gd, etc. [2] for further improving the high-temperature performance of Mg alloys.

Mg alloys with an Nd addition exhibit a strong age-hardening response and improvement in mechanical properties. The precipitation of β″, β′ and β phases and the mechanical properties of some Mg–Nd based alloys have been extensively investigated [3–12]. However, the high-temperature mechanical properties of these Mg–Nd based alloys are often not ideal for applications above 250 °C. Y is an important alloying element to effectively improve the mechanical properties of Mg alloys at elevated temperatures [13–18]. Several important commercial Mg alloys, such as WE54 and WE43, were developed having a combined high-level addition of Y and Nd [13–15]. The precipitation phases in these Mg alloys are β″, β′, β_1 and β, proposed with stoichiometry of Mg_3RE, Mg_5RE, Mg_3RE and Mg_3RE, respectively [14,16]. They provide strengthening effects to these high-Y-containing Mg alloys [13–17].

The addition of Y in high quantities, even for WE54 (Y: 4.75–5.5 wt.%) and WE43 (Y: 3.7–4.3 wt.%) alloy, has the drawbacks to increase alloy density and production cost. Consequently, a lower level addition of Y becomes more attractive if it can produce effective improvements in the mechanical properties of Mg alloys. Recently, a micro-alloy addition of only 1–2 wt.% Y into Mg–3Nd–0.5Zn–0.4Zr (wt.%) alloy has been reported to remarkably increase its tensile properties and creep resistance [18]. It is generally believed that the improvement of the alloy strength is correlated with an enhanced precipitation by the addition of Y. To date, there is a lack of detailed information about the

* Corresponding author at: Australian Centre for Microscopy and Microanalysis, The University of Sydney, Madsen Building F09, Sydney, NSW 2006, Australia. Tel.: +61 2 90369050; fax: +61 2 93517682.
E-mail address: gang.sha@sydney.edu.au (G. Sha).
[1] Present address: Chair of Casting Research, The University of Leoben, A-8700 Leoben, Austria.

0921-5093/$ – see front matter © 2012 Elsevier B.V. All rights reserved.
doi:10.1016/j.msea.2012.01.043

evolution of precipitates microstructure, and the partitioning of solutes into precipitates during ageing low-Y-containing alloys. Better understanding precipitates microstructure formation is of importance for establishing the relationship between the microstructure and mechanical properties of the low-Y-containing Mg–Nd based alloys.

This paper aims to report the mechanical properties and precipitates microstructure of an Mg–2.8Nd–0.6Zn–0.4Zr (wt.%) alloy with a 0.2 wt.% Y addition. By unveiling comprehensive structural and chemical information of solute-rich features formed in the alloy using careful TEM characterisations and quantitative atom probe data analyses, this investigation has objectives to elucidate the precipitation sequence, to address the solute partitioning behaviors during ageing, and to understand the strengthening effect and mechanisms of the low-Y-containing Mg–Nd based alloy.

2. Experimental material and procedures

Mg–2.8Nd–0.2Y–0.6Zn–0.4Zr alloy (wt.%) was prepared with high purity Mg (99.9%), Zn (99.9%), Nd (99.9%), Mg–28Y and Mg–33Zr master alloys in an electric resistance furnace under the protection of an anti-oxidizing flux (containing 54–56% KCl, 14–16% $BaCl_2$, 1.5–2.5% MgO, 27–29% $CaCl_2$), and casted into a sand mould. The chemical compositions of the experimental alloy were determined by using an inductively coupled plasma atomic emission spectrum (ICP-AES) apparatus. The solution treatment of specimens cut from the alloy ingot was conducted at 525 °C for 18 h in a salt bath. The ageing of water-quenched specimens was performed in an oil bath for various ageing time at 200 °C. The Vickers hardness testing was undertaken on LECO Hardness Tester (LV700AT) with 1 kg load and 10 s dwelling time. Each data point reported in this paper represented an average of at least 10 measurements. The tensile tests were performed using standard tensile testing machine (Instron1195) at room temperature (RT), 200 °C, 250 °C, 300 °C and 350 °C, respectively, with a crosshead speed of 5 mm/min and a strain rate of $2.0 \times 10^{-3}\,s^{-1}$. A 5 min holding was applied to each sample to balance its temperature before each high-temperature tensile test. Each data point reported in this paper was an average of at least 3 test samples.

TEM foil specimens were prepared by twin-jet electro-polishing in a solution of 25% $HClO_4$ and 75% methanol at −40 °C and 20 V, and then using low-energy ion beam thinning for surface cleaning. The TEM observations were performed in a Philips CM12 operating at 120 kV and a high resolution TEM (JEOL-3000F) operating at 300 kV. The samples for atom probe analysis were prepared by two-stage electro-polishing of blanks with a size of approximately 0.5 mm × 0.5 mm × 15 mm. The first step was conducted using an electrolyte of 25% perchloric acid in acetic acid at 15 V at room temperature and the second step was in 2% perchloric acid in 2-butoxyethanol at 20 V. Atom probe analyses were performed using a Imago LEAP™ 3000 SI, operating at a specimen temperature of 20 K, 20% voltage pulse fraction and under ultrahigh vacuum conditions (about 1.8×10^{-11} Pa).

Atom probe data sets were carefully reconstructed using an approach outlined recently by Moody et al. [19]. The maximum separation algorithm was employed to identify solute-rich features [20,21], in which Nd and Zn were selected as clustering solutes, a solute-separation distance of 0.8 nm and the minimum size of 15 solute atoms were used in the identification of solute-rich features, such as clusters and precipitates. Solute-rich features containing <15 solutes were neglected in the analysis because such small-size features highly existed in the volume with solutes in random distribution [11,12]. In order to estimate the precise composition of large precipitates, selection-box analysis was employed to measure the composition from the core region of each precipitate in order to reduce the effect of trajectory overlap between precipitate and the Mg matrix on the measurement.

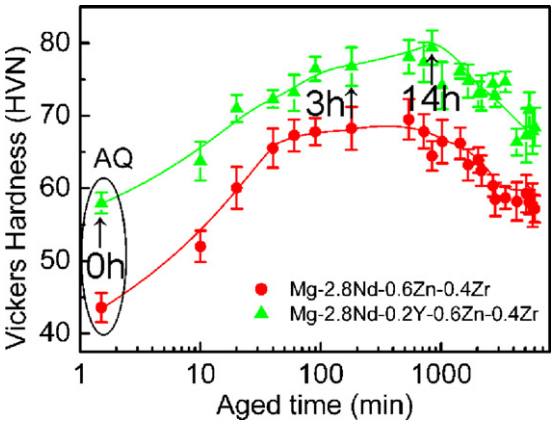

Fig. 1. Age-hardening responses of Mg–2.8Nd–0.2Y–0.6Zn–0.4Zr (wt.%) and Mg–2.8Nd–0.6Zn–0.4Zr alloys aged at 200 °C.

3. Results

3.1. Age hardening response and tensile properties of Mg–Nd–Zn–Zr based alloys

Fig. 1 shows the age-hardening response of two Mg–Nd–Zn–Zr alloys with/without a 0.2 wt.% Y addition during ageing at 200 °C. The Mg alloy with an addition of 0.2 wt.% Y exhibited an enhanced strengthening effect in comparison with the Y-free alloy. The hardness of the as-quenched samples increased from 43.6 ± 2.0 HV to 58.0 ± 2.0 HV. After ageing for 3 h at 200 °C, the hardness of both alloys exhibited strong increases of ∼18.8 HV in the Y-containing alloy and ∼23 HV in the Y-free alloy. The peak hardness of the Y-containing alloy was 79.4 ± 2.4 HV after 14 h ageing. Further ageing beyond 14 h led to progressively decrease in their hardness.

Fig. 2 shows the tensile properties of a Y-containing Mg alloy and a Y-free Mg alloy with different thermal history, including as-cast, as-quenched after a solution treatment, aged for 3 h and 14 h at 200 °C. The tensile strengths of the two alloys (Fig. 2a) are correlated well with the age hardening responses of the two alloys (Fig. 1). An addition of 0.2 wt.% Y provided a clear improvement in the yield strengths (YS) of the alloy in all conditions. However, their ultimate tensile strengths (UTS) and ductility between the two alloys showed no significant difference. The yield strength of the as-quenched samples exhibited an improvement from 100 ± 6.4 MPa to 133 ± 7.2 MPa (Fig. 2a). With the increase in ageing time from 3 h to 14 h, both their UTS and YS increased, but their ductility values decreased, as shown in Fig. 2a. Importantly, the Y-containing alloy in the peak-aged condition (T6, 14 h) exhibited an improved YS over that of the Y-free alloy in the temperature range from RT to 350 °C (Fig. 2b). In particular, the YS of the Y-containing Mg alloy at 200 °C is 183 ± 7 MPa, 28% higher than 143 ± 4 MPa, that of the Y-free alloy. In order to gain insight into microstructures producing the interesting strengthening effect to the Y-containing alloy, samples in different aged conditions were selected to perform further TEM examination and APT analysis.

3.2. TEM characterisation of precipitates in an Mg–Nd–Zn–Zr–Y alloy

Fig. 3 shows a representative bright field (BF) [0 0 0 1] TEM micrograph and the corresponding selected area diffraction patterns (SADP) of an as-quenched sample. No precipitates are evident in TEM image, as shown in Fig. 3a. The diffractions in the SADP were

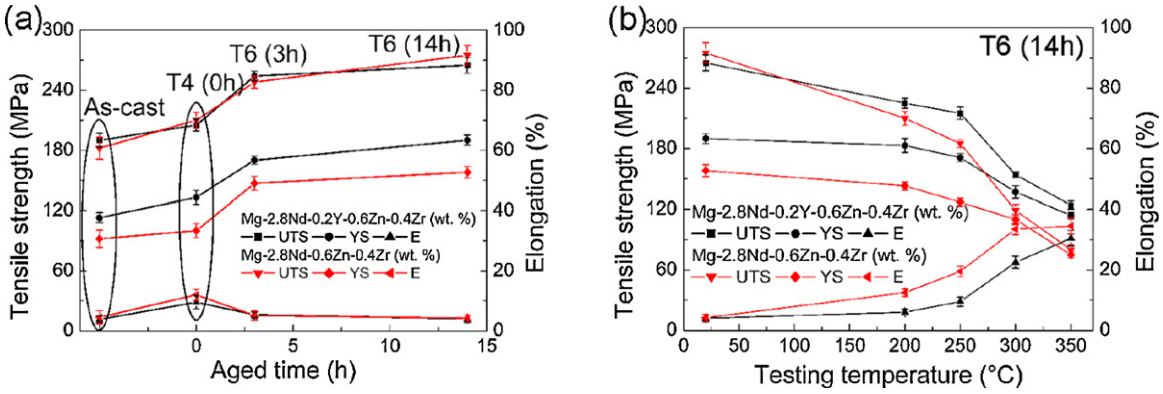

Fig. 2. Tensile properties of Mg–2.8Nd–0.6Zn–0.4Zr (wt.%) alloys with or without 0.2 wt.% Y addition, (a) in different ageing conditions, and (b) measured at different temperatures.

from the α-Mg matrix, as shown in Fig. 3b. The TEM results indicated that no precipitation took place in the as-quenched sample. After aged for 14 h at 200 °C, plate-like precipitates were evident in TEM images, as shown in Fig. 4. The plate-like precipitates habited on $\{1\,1\,\bar{2}\,0\}_\alpha$, and about 16 ± 4.3 nm in length and 1.5 ± 0.7 nm in width with an aspect ratio (length to width) of approximately 10:1, as observed in [0 0 0 1] BF image. The weak diffraction spots at $1/2\{0\,1\,\bar{1}\,0\}_\alpha$ in the [0 0 0 1] SADP, as shown in Fig. 4b, were from β″ precipitates, with $D0_{19}$ structure ($a = b = 0.64$ nm and $c = 0.52$ nm) [14,17]. This was further confirmed by weak diffractions observed at $1/2\{0\,1\,\bar{1}\,0\}_\alpha$ and $1/2\{2\,\bar{1}\,\bar{1}\,4\}_\alpha$ in the $\{2\,\bar{1}\,\bar{1}\,0\}_\alpha$ and $[0\,1\,\bar{1}\,0]_\alpha$ SADPs, as shown in Fig. 4d and f respectively. Weak diffractions at $1/2(2\,\bar{1}\,\bar{1}\,2)_\alpha$ in the $\{0\,1\,\bar{1}\,0\}_\alpha$ SADP, as marked with a white solid arrow in Fig. 4f, suggested that β′ precipitates were present in the microstructure of the alloy. The β′ phase is known to have a base-centred orthorhombic unit cell $a = 0.640$ nm, $b = 2.223$ nm, $c = 0.521$ nm [14,17], and has a lamella-like morphology with a longitudinal axis parallel to $[0\,0\,0\,1]_\alpha$.

The $\{2\,\bar{1}\,\bar{1}\,0\}_\alpha$ and $[0\,1\,\bar{1}\,0]_\alpha$ TEM BF micrographs, as shown in Fig. 4c and e respectively, revealed that thin precipitates (marked with a white solid arrow) habiting on the basal plane of the Mg matrix were present in the microstructure, and they are perpendicular to β-type precipitates (marked with a black solid arrow). No clear streaks of the basal precipitates observed in $[2\,\bar{1}\,\bar{1}\,0]_\alpha$ and $[0\,1\,\bar{1}\,0]_\alpha$ SADPs (Fig. 4d and f) indicated that the basal precipitates were probably at an extremely low volume fraction. The precipitates on basal plane of Mg alloys have been reported to be γ-type phase (γ′, MgZnRE containing, hexagonal, $a = 0.55$ nm, $c = 0.52$ nm [4]). Similar γ-type precipitates were observed in an Mg–Nd–Gd–Zn–Zr alloy aged at 330 °C for 90 min [9].

Careful TEM examinations, as shown in high-resolution TEM images in Fig. 5, revealed that β_1 phase started to appear in the microstructure of the alloy aged for 14 h. The {0 0 2}, {1 1 1} and {2 2 0} lattice planes of a precipitate, as shown in Fig. 5b, were clearly resolved in the high-quality lattice fringe image. The *d*-spacing of {0 0 2}, {1 1 1} and {2 2 0} lattice planes (Fig. 5) were measured to be 0.36, 0.416 and 0.255 nm, respectively, in good agreement with the identification as β_1 phase, with an fcc unit cell ($a = 0.72$ nm), which is very close to $a = 0.74$ nm reported by Nie et al. [14]. The β_1 precipitates were probably at a very low number density in the microstructure, because no clear reflections of β_1 were observed in the SADPs of the alloy, as shown in Fig. 4.

3.3. APT characterisation of precipitates in an Mg–Nd–Zn–Zr–Y alloy

Fig. 6 shows the APT elemental maps of Nd, Y and Zn obtained from an Mg–2.8Nd–0.2Y–0.6Zn–0.4Zr (wt.%) alloy sample quenched in cold water after a solution treatment (for 18 h at 525 °C). A strong clustering of Nd was observed in the Nd atom map, as shown in Fig. 6b. After removing solute atoms in the matrix, fine solute clusters in a high number density, as shown in Fig. 6a, were evident in the analysed volume. No other clear structural feature (i.e. dislocation, precipitates, grain boundary [22]) was

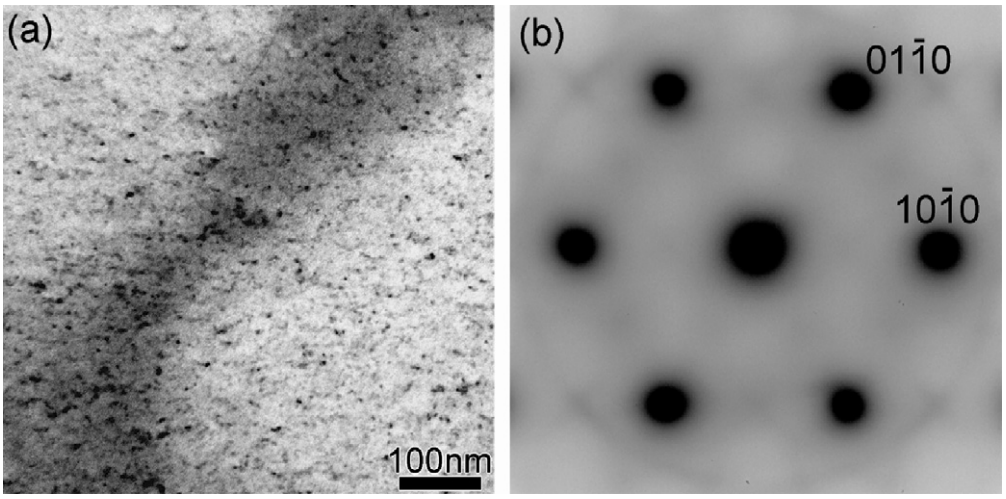

Fig. 3. TEM bright field image in $[0\,0\,0\,1]_\alpha$ zone axis and corresponding SADP of an Mg–2.8Nd–0.2Y–0.6Zn–0.4Zr (wt.%) alloy sample quenched after a solution treatment.

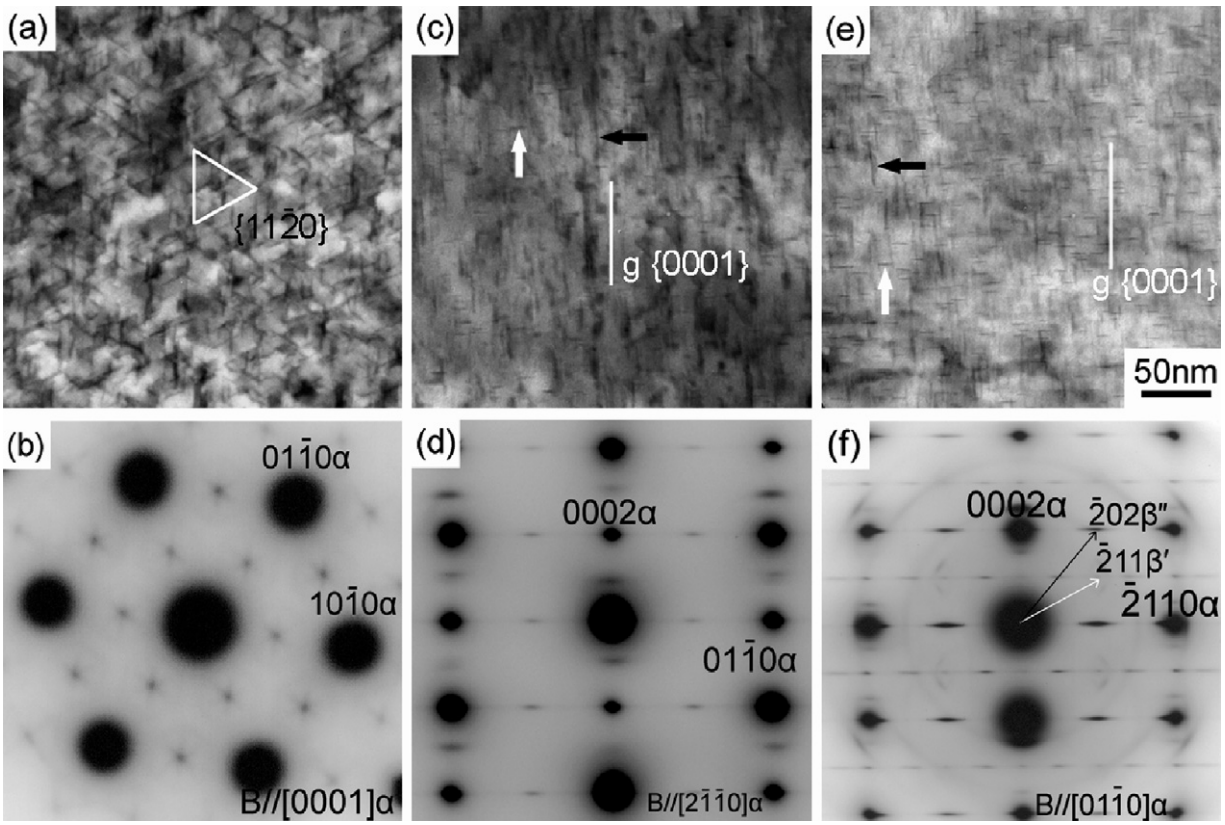

Fig. 4. TEM bright field images and SADPs of the Mg–2.8Nd–0.2Y–0.6Zn–0.4Zr (wt.%) alloy aged at 200 °C for 14 h. (a, b) B//$[0\,0\,0\,1]_\alpha$; (c), (d) B//$[1\ 1\ \bar{2}\ 0]_\alpha$; (e, f) B//$[0\,1\,\bar{1}\,0]_\alpha$.

observed in the analysed volume. After 3 h ageing, platelet precipitates enriched with Nd, Zn and Zr and habited on $\{2\,\bar{1}\,\bar{1}\,0\}$, with an average length of 10 ± 3 nm along $\langle 0\,1\,1\,0\rangle$, were evident within the analysed volume, as shown in Fig. 7. Interestingly, the distribution of Y atoms remained to be uniform and was similar to that observed in the as-quenched condition. After aged at 200 °C for 14 h, the average length of precipitates along $\langle 0\,\bar{1}\,\bar{1}\,0\rangle$ directions were measured to be 15 ± 4 nm, in good agreement with 16 ± 4.3 nm observed by TEM examination in Fig. 4a, and Y remained to be uniformly distributed in the α-Mg matrix, as shown in Fig. 8. Examinations of precipitates in different view directions confirmed that most precipitates were elongated with their longitudinal axis parallel to $[0\,0\,0\,1]_\alpha$, which is in agreement with our TEM observations of β″, β′ and β_1 precipitates. Such precipitates are believed to be effective to hamper the basal dislocation movement [23,24].

The quantitative analysis results of atom probe data are shown in Fig. 9. The number density of the fine solute clusters after solution treatment is $5.0 \pm 0.2 \times 10^{23}$ m^{-3} (which was estimated on the basis of the total number of solute clusters identified in the analysed volume), as shown in Fig. 9a. The number density of solute-rich features reached the peak of $7.6 \pm 0.6 \times 10^{23}$ m^{-3} after 1 h ageing, then decreased significantly to $3.4 \pm 0.6 \times 10^{23}$ m^{-3} (3 h) and further down to $2.4 \pm 0.3 \times 10^{23}$ m^{-3} (14 h) with increasing in ageing time. The solute concentrations of Nd, Zn and Zr in the α-Mg matrix decrease greatly during the ageing up to 3 h, in particular the case

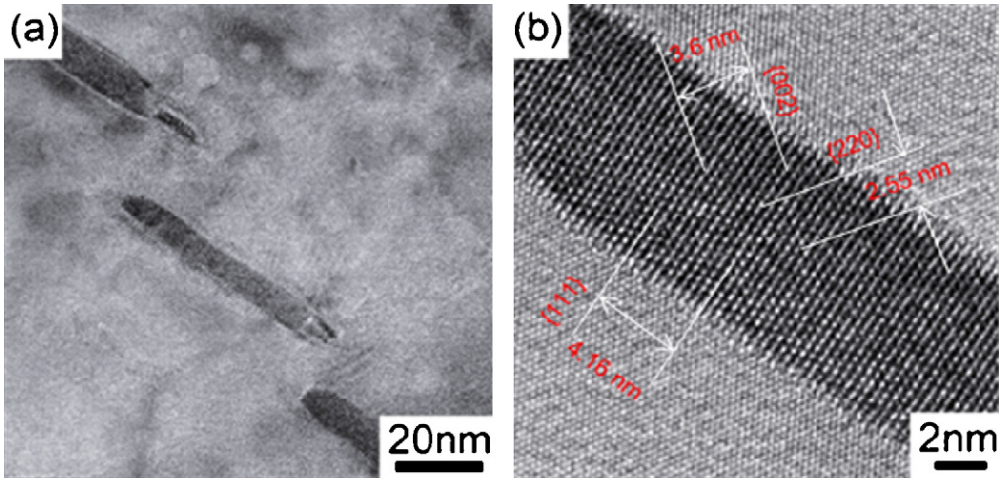

Fig. 5. HRTEM images (a, b) of the precipitates (β_1) in the Mg matrix of an Mg–2.8Nd–0.2Y–0.6Zn–0.4Zr (wt.%) alloy aged at 200 °C for 14 h. B//$[0\,0\,0\,1]_\alpha$.

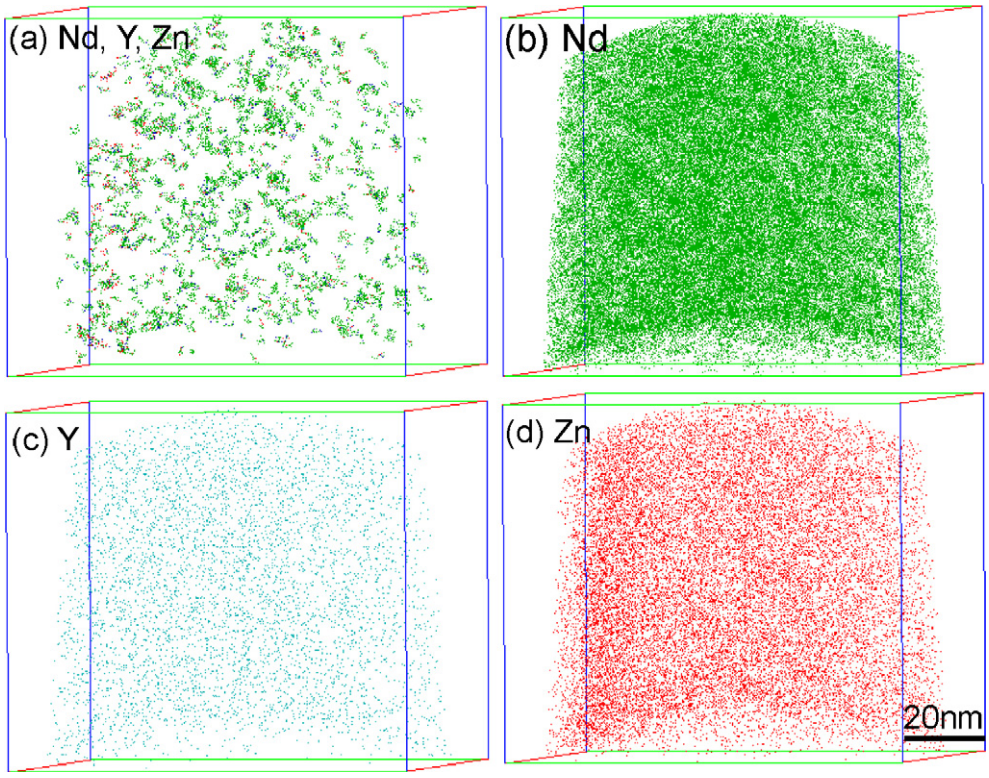

Fig. 6. APT elemental maps of Nd, Y and Zn of an Mg–2.8Nd–0.2Y–0.6Zn–0.4Zr (wt.%) alloy sample quenched after a solution treatment (T4). (a) A combined map of Nd (green), Y (blue) and Zn (red) after removing solutes in the matrix; (b) Nd (green) map; (c) Y (blue) map; (d) Zn (red) map. (For interpretation of the references to color in this figure legend, the reader is referred to the web version of the article.)

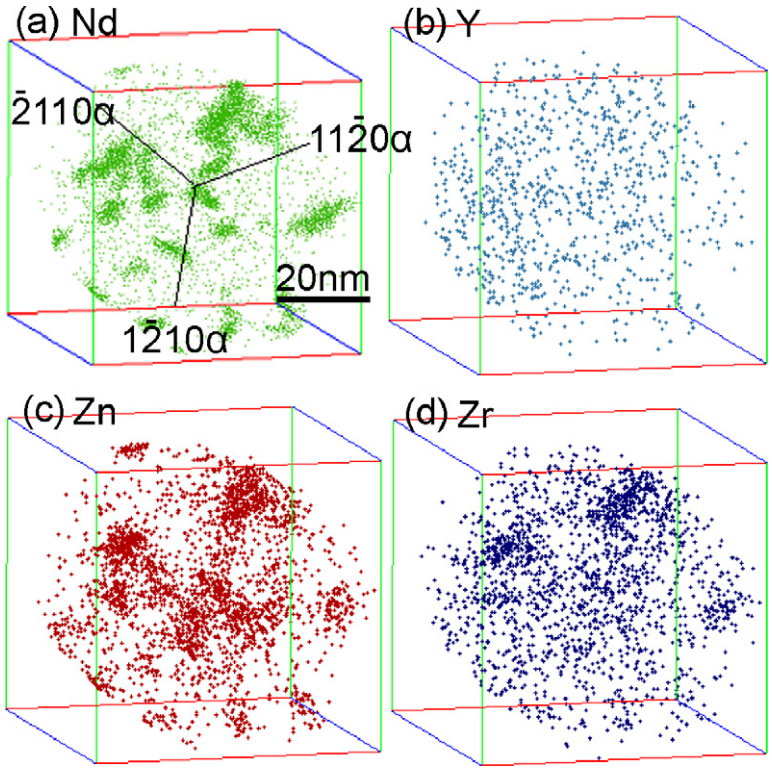

Fig. 7. APT elemental maps of Nd, Y, Zn and Zr of an Mg–2.8Nd–0.2Y–0.6Zn–0.4Zr (wt.%) alloy sample aged at 200 °C for 3 h. (a) Nd (green); (b) Y (light blue); (c) Zn (red); (d) Zr (dark blue). (For interpretation of the references to color in this figure legend, the reader is referred to the web version of the article.)

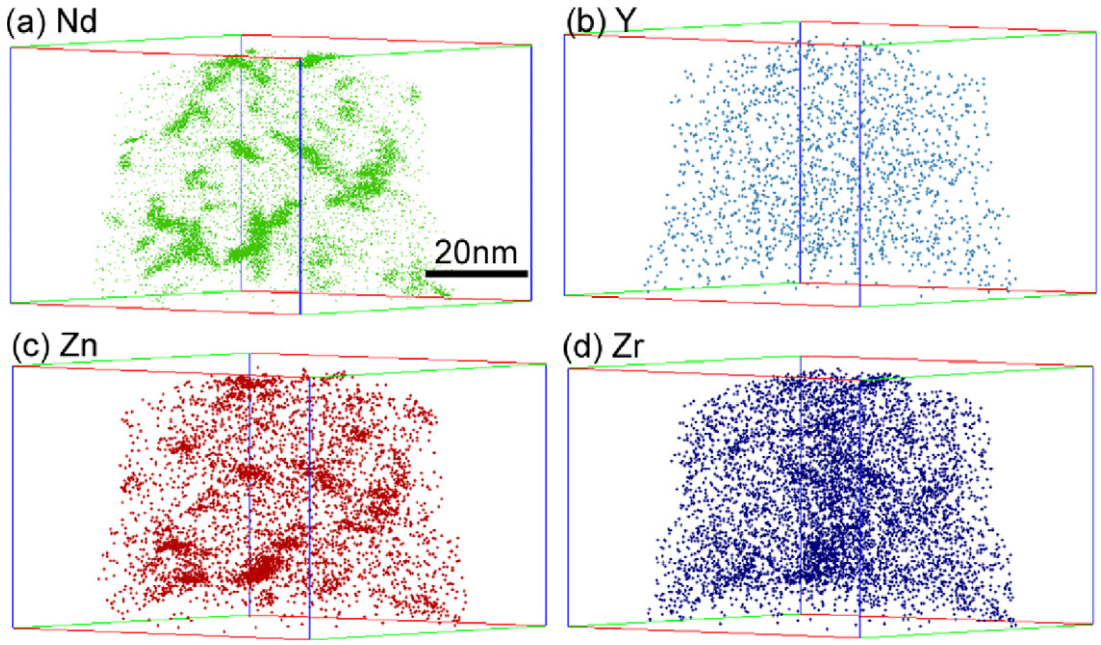

Fig. 8. APT elemental maps of Nd, Y, Zn and Zr of an Mg–2.8Nd–0.2Y–0.6Zn–0.4Zr (wt.%) alloy sample aged at 200 °C for 14 h. (a) Nd (green); (b) Y (blue); (c) Zn (red); and (d) Zr (dark blue). (For interpretation of the references to color in this figure legend, the reader is referred to the web version of the article.)

for Nd, as indicated in Fig. 9b. The decrease of the Nd, Zn and Zr solute concentrations of the matrix is due to the partitioning of these elements into the precipitate, as shown in Fig. 9c and d. The average solute concentration of precipitates increased with the increasing ageing time, as shown in Fig. 9c. The effect of ageing time on partitioning ratio of solutes (calculated by the average solute concentration of precipitates over that of the matrix) is shown in Fig. 9d. Nd was observed having a much stronger partitioning than Zn during the 3 h ageing.

Fig. 10 shows typical composition profiles measured from three different precipitates. The thin precipitates, widely observed in shortly aged samples, contained a low level of solutes and had

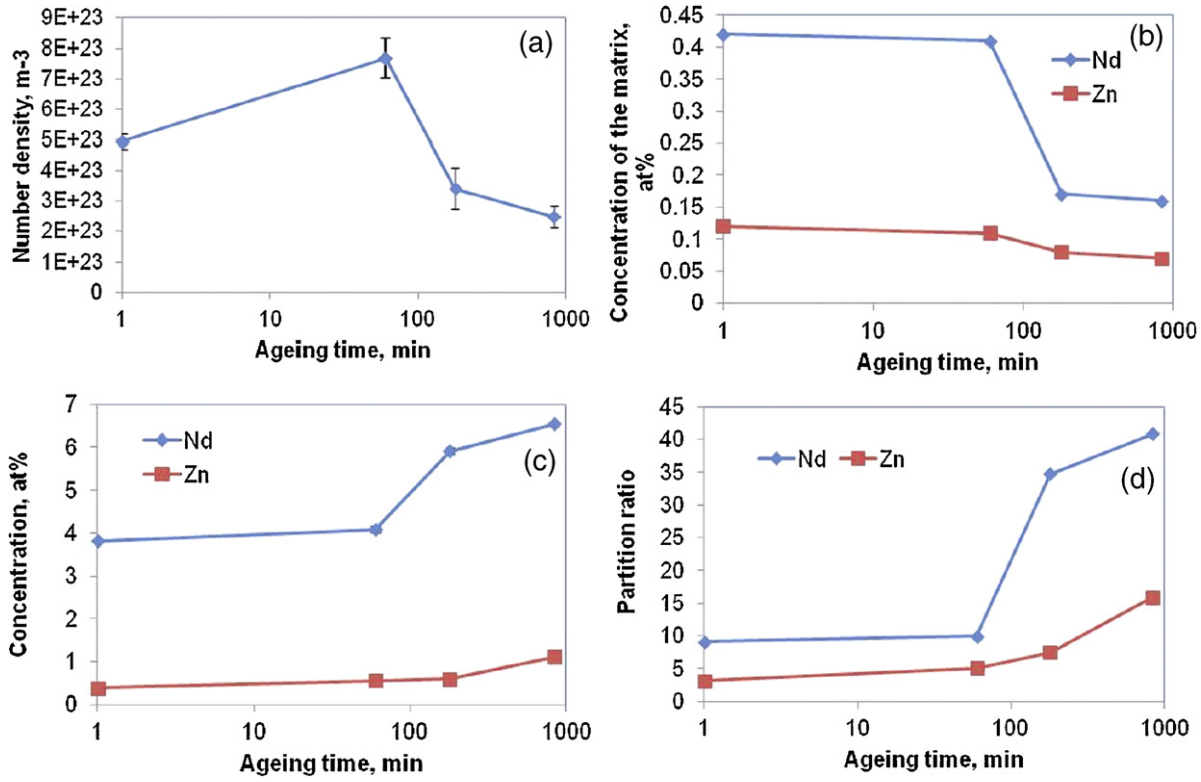

Fig. 9. Quantitative APT analysis results about the evolution of structure and chemical compositions of the solute-rich features and the Mg matrix in Mg–2.8Nd–0.2Y–0.6Zn–0.4Zr (wt.%) alloy during short ageing at 200 °C up to 14 h. (a) number density; (b) solute concentration of the α-Mg matrix; (c) solute concentration of the solute-rich features; and (d) the partitioning ratio of solutes between solute-rich features and the Mg matrix.

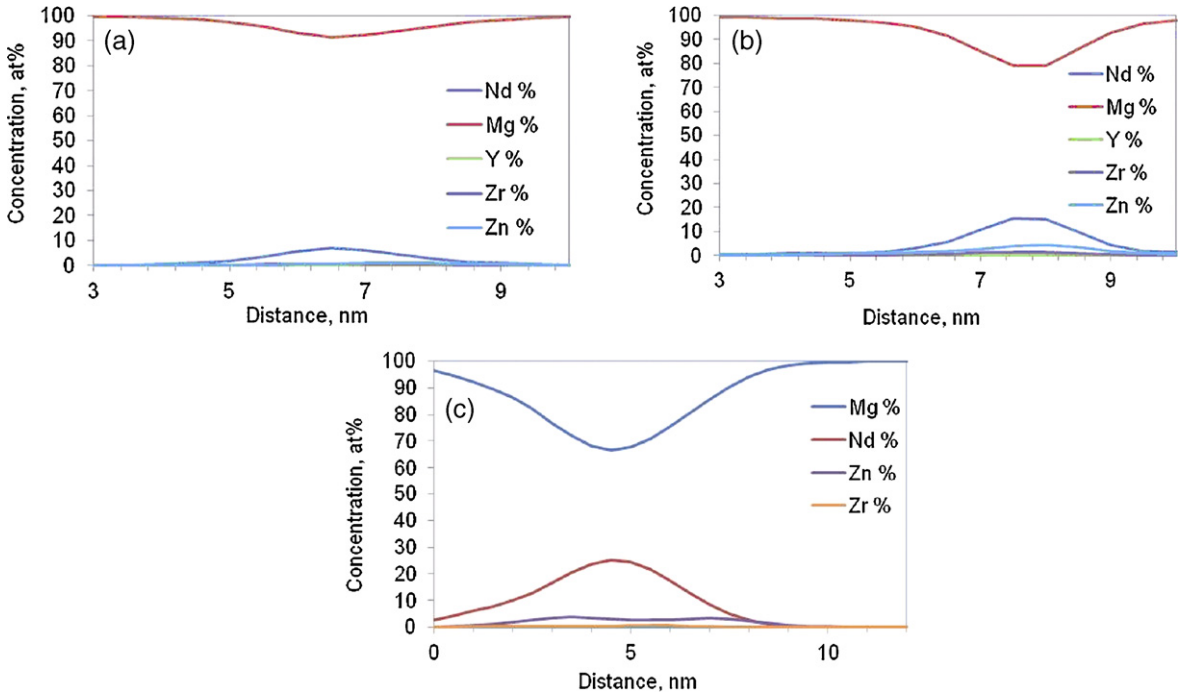

Fig. 10. Typical solute composition profiles measured across the core of three different precipitates in Mg–2.8Nd–0.2Y–0.6Zn–0.4Zr (wt.%) alloy aged at 200 °C for 14 h.

a stoichiometry of Mg_9(Nd,Zn), as shown in Fig. 10a. The thin precipitates likely are β″. The composition profiles of a slightly thicker precipitate, as shown in Fig. 10b, give a stoichiometry of Mg_4(Nd,Zn). Such precipitates were often observed in sample aged for more than 3 h. They are likely β′. A thick precipitate was measured having a core chemistry close to Mg_2(Nd,Zn), as shown in Fig. 10c. It is reasonable to believe that the precipitate is β_1, given that β_1 has been positively identified by TEM characterisation of a 14-h ageing sample (Fig. 5). The different chemical compositions observed among these individual precipitates (Fig. 10) are consistent with the trend observed in Fig. 9c, in which the average solute concentration of solute-rich features increases with increasing ageing time. It is worth noting that the precipitate chemistry unveiled by this work is different from Mg_3RE, Mg_5RE ($Mg_{12}NdY$), Mg_3RE ($Mg_{14}Nd_2Y$) for β″, β′ and β_1 respectively reported in a different Mg alloy [14]. It is unclear if the difference is due to the influence of the alloy composition, ageing condition, or different analysis techniques used. Thin basal γ-type precipitates were not resolved by the APT analysis. This is probably due to the high local magnification effect of the precipitates and the APT detection efficiency of ~55%.

4. Discussion

4.1. Solute clustering and its strengthening effect during the early-stage precipitation in Mg–Nd based alloys

The solute clustering often occurs during the early-stage ageing prior to the formation of precipitates (such as β″ phase [11]), and can affect age-hardening response of various alloys [11,12,25,26]. Our APT characterisation unveiled that Nd was a strong-clustering alloying element and contributed the formation of fine solute clusters (consisting of Nd and Zn) in the as-quenched Y-containing Mg alloy after a solution treatment, as shown in Fig. 9c. The cluster number density in the Y-containing alloy was $5.0 \pm 0.2 \times 10^{23}$ m^{-3}, much higher than $0.2 \pm 0.22 \times 10^{23}$ m^{-3} in an as-quenched Mg–Gd–Nd–Zn–Zr alloy [11,12]. This indicates that the Y addition has promoted the clustering of solutes in the Mg alloy. Interestingly, no clear Y clustering was detected during the early clustering of solutes as shown in Fig. 6c. The precise reason for the enhanced Nd clustering in the Mg alloy with a Y addition is unclear, which is probably correlated with the effect of Y addition on the solubility of Nd in Mg and the enhanced diffusion of Nd due to its high binding energy with vacancies (0.25 eV) [27]. It is worth-noting that although the number density of solute clusters in the Mg alloy is closer to that observed in some Al alloys [22,25,26], it should not be a surprise that the strength of this Mg alloy is much lower than those of the Al alloys since the deformation mechanisms of Mg alloys are greatly different from those of Al alloys. In addition, not all solute clusters are able to provide the same strengthening effect even in Al alloys [25]. The significant enhanced strength (from 43 HV to 58 HV in hardness, and from 100 MPa to 133 MPa in YTS) of the Y-containing alloy above that of the Y-free alloy, as shown in Figs. 1 and 2, clearly indicated that the solute clusters did provide effective strengthening effect to the Y-containing Mg alloy.

4.2. Precipitates and their strengthening effect in the Mg–Nd–Y–Zn–Zr alloy

The precipitation sequence of β-type precipitates in the low-Y-containing Mg–Nd based alloy is: solute clusters → β″ → β′ → β_1 during the ageing up to 14 h according to our TEM and APT characterisations. γ-Type precipitates were observed in the alloy. The basal γ-type precipitates are known to be less effective to hinder the sliding of dislocations on basal planes, and are less effective to provide strengthening effect than prime β-type precipitates in Mg alloys at room temperature [23]. With increasing ageing time, the size and chemical composition of β-type precipitates, as shown in Figs. 7–9, increased. Meanwhile, there was further enhanced partitioning of Nd and Zn into precipitates with the increasing ageing time from 1 h to 14 h, as shown in Fig. 9c and d, which were correlated well with the formation of more β′and β_1 precipitates containing higher concentrations of Nd and Zn, as shown in Fig. 10.

With the increase in ageing time, the number density of solute-reach features reached the peak value in the alloy at 1 h ageing and decreased progressively thereafter. The increase in number density

of solute-rich features (including clusters and small β″ precipitate) provided further strengthening to the alloy, with a hardness increase of 15 HV, as shown in Fig. 1. A decrease of the number density of solute-rich features (Fig. 9a), but an additional hardness increase of 7 HV (Fig. 1) in the alloy during further ageing up to 14 h, indicated that volume fraction of solute-rich features are important for producing strengthening effect. More information about the effect of precipitate volume fraction on the precipitation-strengthening can be found in Ref. [28].

Many Mg alloys have been observed to form precipitates in a high number density, similar to that observed in our Y-containing Mg alloys, but different age-hardening response. For example, a hot-rolled Mg–12Gd–1.9Y–0.69Zr alloy aged at 200 °C was reported to produce solute-rich features in the order of 10^{24} m^{-3} in a number density [16], higher than that observed in our cast Y-containing Mg alloy. The wrought alloy was reported to have the peak hardness of 130 HV, much higher than that of our cast alloy. This is likely due to the high content of alloying elements and refined grain size of the wrought Mg alloy. In contrast, WE43 alloy was reported to have precipitate number density of 1.5×10^{24} m^{-3} and the peak hardness of 100 HV [29], which is much close to that of our Y-containing Mg alloy. In literatures, some Mg alloys, such as AZ91 alloy [30], were reported having similar hardening response as our Y-containing Mg alloy, but much lower number density of precipitates (1.09×10^{19} m^{-3}) than that of our Y-containing Mg alloy. The low-number-density measurement could often found to be related with the different analysis technique used in their measurement. Our TEM and APT characterisation of the as-quenched samples (Figs. 3 and 6, respectively) clearly demonstrated that fine solute clusters easily identified by APT are hard to be resolved by TEM examinations. As a result, TEM examinations could easily underestimate the number density of solute-rich features in the microstructure. In order to make a sensible comparison among results obtained by different analysis techniques, the limitations of each analysis technique have to be taken into consideration. This indeed creates some difficulties to correlate with results obtained by different analysis techniques. To better understanding age-hardening response of AZ91 alloy, some detailed APT characterisation will be useful.

The Y-containing alloy aged for 14 h at 200 °C was observed having the co-existence of β-type prismatic precipitates and γ-type basal precipitates in the microstructure, as shown in Fig. 4. Single type precipitates, either β-type or γ-type, were frequently observed in many Mg alloys. For example, β-type precipitates were observed in the Mg–RE alloys [9,14,17]. The γ-type thin basal precipitates have been observed in Mg–8Y–2Zn–0.6Zr (wt.%) alloy [31], Mg–1Gd–0.4Zn–0.2Zr (at.%) alloy [32], Mg–2.4Nd–0.4Zn–0.6Zr (wt.%) alloy [5] and Mg–2.8Nd (wt.%) alloy with the addition of 1.3 wt.% Zn [3,4]. However, to our knowledge, the simultaneous co-existence of β-type precipitates and γ-type precipitates has not been reported in previous studies of Mg–Nd based alloys, although co-existence of precipitates lying either parallel to the basal plane or at an angle to basal plane have been reported in AZ91 alloy [30]. It is worthnoting that the two types of precipitates can produce different strengthening effects. The basal γ-type precipitates are effective to serve as obstacles for non-basal slipping of dislocations, and hence improve the high-temperature mechanical properties of Mg alloys [33]. The formation of γ-type precipitates in the Mg–2.8Nd–0.2Y–0.6Zn–0.4Zr (wt.%) alloy (Fig. 4) was consistent with the improved yield strength of the alloy at elevated temperatures (Fig. 2b). The prismatic β-type precipitates in the alloy are believed to play an important role to enhance alloy's mechanical properties at room temperature. TEM observation (Figs. 3–5) and atom probe tomography (Figs. 7 and 8) revealed a high number density of plate-shape β series precipitates formed on prismatic planes of the α-Mg matrix during ageing treatment. To date, it is unclear why two types of precipitates formed simultaneously in the alloy. More fundamental research is necessary to unveil factors controlling the formation of two types of precipitates. This will be important for design and developing new advanced Mg alloys with excellent performance at room temperature and elevated temperatures.

5. Summary

1. A new Mg–2.8Nd–0.6Zn–0.4Zr (wt.%) alloy with 0.2 wt.% Y addition showed a significant improvement on hardness and tensile properties during ageing at 200 °C for up to 14 h. The alloy, in particular, exhibited enhanced tensile yield strength in the temperature range of 200–350 °C.
2. The low-level Y addition has promoted the significant clustering of Nd and Zn, and subsequently the formation of high-number-density β-type precipitates with Nd, Zn and slight Zr enrichments.
3. The partitioning of Nd into β-type precipitates in the alloy was much stronger than other alloying elements. Interestingly, the distribution of Y atoms remained in the alloy with increasing in ageing time, without exhibiting any significant partitioning into precipitates in the alloy during ageing at 200 °C.
4. The improvement of mechanical properties at elevated temperatures was correlated well with an enhanced precipitation of β-type precipitates, including β″, β′ and β_1, and the co-existence with basal γ-type precipitates in the microstructure of the alloy.
5. The stoichoimetry of β″, β′ and β_1 was measured to be Mg_9(Nd,Zn), Mg_4(Nd,Zn), and Mg_2(Nd,Zn) respectively in the Mg alloy.

Acknowledgments

The authors are grateful for scientific and technical input and support from the Australian Microscopy & Microanalysis Research Facility (AMMRF) node at the University of Sydney. Jiehua Li also wishes to thank the China Scholarship Council for financial support. This work is partly supported by the Doctorate Foundation of Northwestern Polytechnical University under Grand No. (CX200705).

References

[1] I.J. Polmear, Mater. Sci. Technol. 10 (1994) 1.
[2] B.L. Mordike, Mater. Sci. Eng. A 324 (2002) 103–112.
[3] T.J. Pike, B. Noble, J. Less Common Met. 30 (1973) 63.
[4] P.A. Nuttall, T.J. Pike, B. Noble, Metallography 13 (1980) 3–20.
[5] D.H. Ping, K. Hono, J.F. Nie, Scripta Mater. 48 (2003) 1017–1022.
[6] R. Wilson, C.J. Bettles, B.C. Muddle, J.F. Nie, Mater. Sci. Forum. 41 (267) (2003) 9–422.
[7] L.R. Gill, G.W. Lorimer, P. Lyon, Adv. Eng. Mater. 9 (2007) 784.
[8] P.J. Apps, H. Karimzadeh, J.F. King, G.W. Lorimer, Scripta Mater. 48 (2003) 1023–1028.
[9] G. Sha, J.H. Li, W. Xu, K. Xia, W.Q. Jie, S.P. Ringer, Mater. Sci. Eng. A 527 (2010) 5092–5099.
[10] J.H. Li, W.Q. Jie, G.Y. Yang, Trans. Nonferrous Met. Soc. China 18 (2008) s27–s32.
[11] G. Sha, J.H. Li, W.Q. Jie, S.P. Ringer, in: K.U. Kainer (Ed.), Proceedings of 8th International Conference on Magnesium Alloys and their Applications, Wiley-VCH Verlag GmbH & Co. KGaA, Weinheim, 2009, pp. 40–45.
[12] J.H. Li, G. Sha, T.-Y. Wang, W.Q. Jie, S.P. Ringer, Mater. Sci. Eng. A (2011), doi:10.1016/j.msea.2011.10.092.
[13] J.F. Nie, B.C. Muddle, Scripta Mater. 10 (1999) 1089–1094.
[14] J.F. Nie, B.C. Muddle, Acta Mater. 48 (2000) 1691–1703.
[15] C. Antion, P. Donnadieu, F. Perrard, A. Deschampa, C. Tassin, A. Pisch, Acta Mater. 51 (2003) 5335–5348.
[16] T. Honma, T. Ohkubo, K. Hona, S. Kamado, Mater. Sci. Eng. A 395 (2005) 301–306.
[17] T. Honma, T. Ohkubo, S. Kamado, K. Hono, Acta Mater. 55 (2007) 4137–4150.
[18] J.H. Jun, B.K. Park, J.M. Kim, K.T. Kim, Adv. Mater. Res. 26-28 (2007) 137–140.
[19] M.P. Moody, B. Gault, L.T. Stephenson, D. Haniel, S.P. Ringer, Ultramicroscopy 109 (2009) 815–824.
[20] J.M. Hyde, C.A. English, in: R.G.E. Lucas, L. Snead, M.A.J. Kirk, R.G. Elliman (Eds.), Microstructural Processes in Irradiated Materials, MRS 2000 Fall Meeting Symposium, Boston, MA, 2001, p. 27.

[21] D. Vaumousse, A. Cerezo, P.J. Warren, Ultramicroscopy 95 (2003) 215–221.
[22] G. Sha, R.K.W. Marceau, X. Gao, B.C. Muddle, S.P. Ringer, Acta Mater. 59 (2010) 1659–1670.
[23] J.F. Nie, Scripta Mater. 48 (2003) 1009–1015.
[24] C.L. Mendis, C.J. Bettles, M.A. Gibson, C.R. Hutchinson, Mater. Sci. Eng. A 435-436 (2006) 163–171.
[25] R.K.W. Marceau, G. Sha, R. Ferragut, A. Dupasquier, S.P. Ringer, Acta Mater. 58 (2010) 4923–4939.
[26] R.K.W. Marceau, G. Sha, R.N. Lumley, S.P. Ringer, Acta Mater. 58 (2010) 1795–1805.
[27] T. Gorecki, in: F.J. Kedves, D.L. Beke (Eds.), Proc. Int. Conf. On Diffusion in Metals and Alloys (DIMETA-82), Trans Tech Publications, Switzerland, 1983, p. 365.
[28] S. Esmaeili, D.J Lloyd, Acta Mater. 53 (2005) 5257.
[29] G. Barucca, R. Ferragut, F. Fiori, D. Lussana, P. Mengucci, F. Moia, G. Riontino, Acta Mater. 59 (2011) 4151–4158.
[30] S. Celotto, Acta Mater. 48 (2000) 1775–1787.
[31] Y.M. Zhu, A.J. Morton, M. Weyland, J.F. Nie, Acta Mater. 58 (2010) 464–475.
[32] J.F. Nie, K. Oh-ishi, X. Gao, K. Hono, Acta Mater. 56 (2008) 6061–6076.
[33] A. Galiyev, R. Kaibyshev, G. Gottstein, Acta Mater. 49 (2001) 1199–1207.